Identification and pairing re-assessment of unequilibrated ordinary chondrites from four Antarctic dense collections areas.

Kevin Righter[1], John Schutt[2], Nicole Lunning[1], Ralph Harvey[2], James Karner[3]

1 – ARES, Mailcode XI2, NASA-JSC, Houston TX, 77058

2 – Department of Earth, Environmental, and Planetary Science, Case Western Reserve University, 10900 Euclid Ave., Cleveland, OH 44106

3 – Department of Geology and Geophysics, University of Utah, Salt Lake City, UT 84113

[submitted to *Meteoritics and Planetary Science*, March 2021]

[revised and resubmitted May 2021]

Abstract – New analyses of Cr_2O_3 contents of olivines from Type II chondrules in un-equilibrated chondrites (UOC) from 4 dense collections are reported here. This survey of petrologic type 3 UOCs was undertaken to identify primitive chondrites that may have been overlooked, and to address possible pairing errors. We have identified 23 primitive UOCs (≤3.10) (only 5 identified previously, for a total of 28 overall), and also recommend other revisions to prior classifications and pairings.

Introduction

Unequilibrated ordinary chondrites (UOC) of petrologic type 3 are scientifically valuable samples whose least-metamorphosed specimens provide important information about the early solar system. For example, UOCs can typically contain metal (Kimura et al., 2008), primitive chondrules (Wasson et al., 1995; Lauretta et al., 2006), pre-solar grains (Nittler et al., 2007; Zega et al., 2014), organics (Alexander et al., 2010; Busemann et al., 2007), nebular materials in matrix (Doyle et al., 2015), and/or isotopic records of the early solar system processes (Telus et al., 2018; Mishra and Goswami, 2014) making their identification of great interest. Determining the relative degree of thermal equilibration in the least metamorphosed of these specimens has been central to chondrite classification since the introduction of the concept of petrologic types 3 to 6 (least to most metamorphosed; van Schmus and Wood, 1967). Within the type 3 chondrites, subtle geochemical and mineralogical changes occur at even modest levels of equilibration, and thus have the potential to obscure characteristics that are truly nebular. Sears et al. (1980) proposed a range of metamorphic properties with the type 3 ordinary chondrites based on thermoluminescence (TL) sensitivity and subdivided type 3 into ten finer divisions: types 3.0

through 3.9 (again least to most metamorphosed within type 3). The ability to identify the lowest petrologic types 3.0 to 3.2 could thus lead to valuable discoveries of nebular materials that might otherwise be overlooked in materials classified simply as type 3.

UOC's can be identified using several different approaches such as natural thermoluminesce or NTL (e.g. Sears et al., 1991; Benoit et al., 2002), Raman spectra of polyaromatic carbon (Bonal et al., 2016), FeNi metal textures and composition (Kimura et al., 2008), and Cr content in olivine from Type II chondrules (Grossman and Brearley, 2005). One of the first examples of UOCs from Antarctica was the ALH 77011 pairing group identified by Scott (1984) and later studied in greater detail with NTL by Sears et al. (1991). This group comprises >70 samples, and the challenges involved with pairing them as a single group versus multiple groups are discussed in those studies. Most of these are L3.4 to L3.6, where in spite of few readily visible textural changes, significant geochemical equilibration has occurred, making them less valuable for nebular studies than more primitive chondrites. Similarly, the lack of obvious textural distinctions between many low-petrographic-type Antarctic samples led classifiers to pair numerous samples in the 1990s. Pairing groups from dense collections areas (DCA) are common but often only become evident over time and thus need to be re-evaluated regularly. More detailed follow-up studies have identified more primitive materials within these pairing groups, sometimes leading to the reclassification of one or more specimens (e.g., Bonal et al., 2016; Benoit et al., 2002). Identification of such new material is exciting, but has rarely included the systematic examination of all members or all specimens from one area.

With the goal of discovering previously un-identified specimens of low-petrographic-type we have systematically examined large L3.x pairing groups from the Meteorite Hills (MET), Elephant Moraine (EET), Lewis Cliffs (LEW), and Grosvenor Mountains (GRO) areas.

Using standard microprobe analysis of olivines from Type II chondrules, we have undertaken surveys of Cr in olivine from these groups to identify the most primitive L3s from these areas and re-examine the pairing accordingly. Grossman and Brearley (2005) showed that the Cr content of ferroan olivine is an extremely sensitive indicator of metamorphic grade in low petrographic-type chondrites. At the time of accretion, ferroan olivine in ordinary chondrites had elevated Cr contents, most likely due to rapid cooling during chondrule formation. During the initial stages of metamorphism, Cr exsolved from olivine, causing precipitation of fine-grained chromite. Further heating caused coarsening of chromite into equant grains, interior to and rimming olivines. These changes at low petrologic type make Cr contents of olivine an excellent classification tool for chondrites of types 3.0–3.2 (Grossman and Brearley, 2005). Using these new olivine analyses, we have identified many previously unrecognized 3.00-3.05 UOC and have proposed new pairing relations for others.

Samples and analytical approach

Thin sections analyzed for this work were either the JSC library section or, if available, a larger-area section that would allow analysis of the most possible olivine grains. The thin section numbers (TS#) for each meteorite sample are listed in **Tables 1-4**. Chemical analyses of the olivines in the unequilibrated ordinary chondrites were made by wavelength dispersive X-ray spectroscopy using a Cameca SX100 electron microprobe at NASA-JSC, with an accelerating voltage of 15 kV, a beam current of 20 nA, and peak counting time of 60 sec. The standards used for silicate and oxide analyses were chromite (Cr), rutile (Ti), rhodonite (Mn), oligoclase (Na, Al), Marjalahti pallasite olivine (Mg), fayalite (Fe), diopside (Ca), and natural glass K411 (Si, Al). Detection limits for minor elements TiO_2, Al_2O_3, Cr_2O_3, MnO, NiO, and CaO were 0.01

wt%. Typically 30 to 50 random points on FeO-rich chondrules in one thin section were analyzed and a mean and 1 sigma (σ) calculated for each sample (**Tables 1-4**).

Results

The olivine microprobe analyses from each sample were used to calculate σ–Cr_2O_3, and then plots constructed of Cr_2O_3 versus σ–Cr_2O_3, and compared to the sub-fields defined by Grossman and Brearley (2005) (**Figure 1**). The new analyses in many cases fall outside of the boundaries from Grossman and Brearley (2005), suggesting the position of the metamorphism trends may vary from those originally defined in that work. This has been recognized in other studies as well (e.g., Simon and Grossman, 2015; Davidson et al., 2014). In cases where our analyses fall off the original trendline (or metamorphic curve) of Grossman and Brearley (2005), we assigned sub-types by extending the dashed lines that are orthogonal to the curve. Therefore, the 3.00 have low σ–Cr_2O_3 values, and then as metamorphism proceeds σ–Cr_2O_3 values increases to higher values while remaining at similar Cr_2O_3 (beginning of Cr in olivine exsolution), and then finally σ–Cr_2O_3 and overall Cr_2O_3, decrease forming a positive correlation to higher degrees of metamorphism as Cr_2O_3 is lost to chromite and the σ–Cr_2O_3 values decrease with homogenization (Grossman and Brearley, 2005).

Several samples were analyzed by both Grossman and Brearley (2005) and our study, allowing comparison of results. EET 90161 exhibits high Cr_2O_3 (0.43) and moderate to high σ–Cr_2O_3 (0.09), although our study found slightly lower values than Grossman and Brearley (2005) with Cr_2O_3 = 0.50 and σ–Cr_2O_3 = 0.21. The MET 96503 olivines yielded nearly identical values of Cr_2O_3 (0.32) and σ–Cr_2O_3 (0.22) to those reported by Grossman and Brearley (2005) (Cr_2O_3 = 0.31 and σ–Cr_2O_3 = 0.22). Similarly, the MET 00526 olivines yielded nearly identical

values of Cr_2O_3 (0.48) and σ–Cr_2O_3 (0.16) to those reported by Grossman and Brearley (2005) (Cr_2O_3 = 0.47 and σ–Cr_2O_3 = 0.16). Finally, GRO 95544 and 95502 both yielded lower Cr_2O_3 (0.08-0.12) and σ–Cr_2O_3 (0.05-0.07) both in agreement with those values reported by Grossman and Brearley (2005) (Cr_2O_3 = 0.08 and σ–Cr_2O_3 = 0.05-0.06).

For each DCA there is a map (**Figures 2, 3, 4 and 5**), a Cr in olivine plot (**Figure 1**), and a table of analytical results for olivine (**Tables 1-4**). These will be called out in the text for clarity.

Elephant Moraine (EET) [1]

Twenty-one L3 chondrites were recovered from the Elephant Moraine (EET) icefields in the 1982, 1983, 1987, 1990, 1992, and 1996 field seasons (**Figure 2**). Only a few have been paired together, such as EET 90080-90161-90261, and classified initially as L3.4. Benoit et al. (2002) and Grossman and Brearley (2005) identified EET 90161 as a primitive L3.05-3.1. Benoit et al. (2002) also measured EET 90066 and 90628—they suggested the former is 3.05 and the latter is 3.4. Meanwhile, Bonal et al. (2016) suggested on the basis of Raman spectroscopy that EET 87735, 90066, 90628, and 90909 are all 3.05-3.1, and 90083 is 3.1-3.4, while 82601 is 3.5-3.7. Given the suggestion that many samples could be more primitive than L3.4, we have undertaken a survey of 17 samples using Cr in olivine approach of Grossman and Brearley

[1] **Notes on Icefield Naming:** Antarctic meteorites are typically recovered from areas of exposed blue ice high on the East Antarctic icesheet, with those in the US collection assigned a formal name that includes a 3-letter prefix representing a nearby geographical feature. Unfortunately, the scarcity of named features on the icesheet combined with the expansive and often discontinuous nature of some blue ice areas can mean that specimens bearing the same prefix often were recovered from sites as many as 50 km apart. This is the case for several of the pairing groups in our study. The EET specimens, for example, can originate from several geographically-distinct blue ice areas associated with the Elephant Moraine (the only named feature in this region). Where possible we have used the informal names for these distinct icefields (used by ANSMET field parties) to help specify the geographical location of specimens. For the EET region these include Meteorite City, Texas Bowl and the Northern Ice Patch as well as the main Elephant Moraine icefield. Specimens from icefields in the Grosvenor Mountains (GRO) region are similarly designated with informal names to better distinguish those from the Mt. Bumstead, Block Peak/Mauger Nunatak/ Mt. Block and Mt Cecily-Raymond icefields.

(2005). Indeed, there are 12 members of this group that are 3.00-3.15, and based on the find locations and detailed olivine compositions, below we propose new pairings for these samples (**Figure 1 and Table 1**).

Lewis Cliffs Ice Tongue (LEW)

A similar situation exists for L3 chondrites from the Lewis Cliffs Ice Tongue (LEW) area that include a total of 57 meteorites from the 1985, 1986, 1987, 1988, 1992, and 1997 seasons, with numerous small groups proposed as paired (**Figure 3**). Sears et al. (1991) identified LEW 86134, LEW 86018, LEW 86549 and LEW 86207 as potentially primitive based on their NTL, and LEW 86134 was confirmed with Cr in olivine studies of Grossman and Brearley (2005). Bonal et al. (2016), on the other hand, suggested LEW 87208 is primitive, while suggesting LEW 86018, LEW 86549 are 3.4 and 3.6, respectively. Given the potential for finding primitive members amongst this large group of L3s, and also the disagreement between previous studies in identifying the most primitive samples, we have undertaken a systematic survey of 49 LEW L3s using the Cr in olivine approach. We have confirmed the primitive nature of LEW 86134, while also identifying LEW 97202 and LEW 87208 as L3.00 to 3.05 (**Figure 1 and Table 2**). Some identified in previous work as potentially primitive have low Cr in olivine (e.g., LEW 86018 and LEW 86207) and thus are not as primitive as LEW 86134, LEW 87208, and LEW 94202. All other LEW UOCs studied here are of petrologic type 3.15 or higher.

Grosvenor Mountains (GRO)

Fifteen L3 meteorites have been recovered from the Grosvenor Mountains (GRO) area, with twelve of them from the Mt. Cecily-Mt. Raymond area (**Figure 4a**) and four others from the

Otway, Bumstead, and Mt. Block-Mauger-Block Peak areas (**Figure 4b**). GRO 95502, 95504, 95505, 95512, 95536, 95539, 95544, 95545, and 95546 were all measured for NTL, revealing low values suggesting primitive 3.1 material. Grossman and Brearley (2005) examined Cr in olivines from 95502 and 95504 and suggested 3.1/3.2 for these two samples. Bonal et al. (2016) also found a wide range from 3.1 to 3.5 represented within members of this group, as well as a very primitive sample GRO 06054 – L3.05, based on Raman spectral analyses. Due to the dispersion of results and the large number and size of samples from GRO, we have again undertaken a systematic survey of Cr in olivines from these fifteen samples. The results are surprising and reveal a range of petrologic types, including four primitive UOCs (GRO 95558, GRO 06054, GRO 03015 and GRO 03061). All other GRO samples from this group appear to be of petrologic type 3.2 or higher (**Figure 4 and Table 3**).

Meteorite Hills (MET)

The Meteorite Hills (MET) area yielded many low petrologic type ordinary chondrites in the 1996, 2000, and 2001 seasons (**Figure 5**), many of which were initially classified as L3.4 to L3.6. Benoit et al. (2002) found low NTL values for MET 96503 and MET 96515 indicating these two samples could be as low as L3.0-3.1. Detailed analysis of olivine composition revealed several groups, with one comprised of primitive chondrites (3.05 and 3.10; MET 00452 and MET 00526, Grossman, personal comm.), and MET 96503 (L3.1/3.2). Bonal et al. (2016) confirm the low petrologic type for MET 00452 and 00526, as well as the previous suggestions for MET 96503 and 96515. They also suggested MET 00489, originally classified as L3.6, is of primitive nature. Given that there are >15 L3s from this region, we have undertaken a systematic survey of this region and combined our data with previous work (Grossman and Brearley, 2005;

Grossman, unpublished). From these combined results, we suggest multiple pairing groups for the MET region. Our results confirm the primitive nature of MET 00452 and 00526, and suggest that MET 00621 be included with this pairing and L/LL3.05. The L3 chondrites MET 96503, 96515, 01051, 01056, and 01057 all have lower Cr_2O_3 contents in the olivine and appear to be L3.10 to 3.15. The H3 chondrites MET 00506, 00552, and 00607 have similar and low Cr_2O_3 contents in the olivine and appear to be H3.10. And finally, MET 01182, 00570, and 00489 all have very low Cr_2O_3 contents (< 0.09 wt%) and are consistent with their current classifications of 3.6 or higher petrologic type.

Discussion

Pairing is a difficult task as has been identified and highlighted by previous workers (Marvin, 1989; Benoit et al., 2000; Welten et al., 2001). Proximity of find is a major and pragmatic component of pairing, but is subject to interpretation. Paired samples can be the result of a single sample being broken up into multiple pieces after hitting the ice or snow and being dispersed by ice flow, wind transport, or weathering in general. Pairing groups can also originate from a strewnfield, where multiple meteorites have fallen at the same time as part of a shower. Such a strewnfield can then become distorted or modified by ice flow or wind transport. It must be remembered that many Antarctic meteorites have long histories in or on the icesheet. Terrestrial ages of meteorites in excess of 500,000 years have been reported from the Lewis Cliff and other meteorite stranding sites in the Beardmore region. (Welten et al., 1999). These dense accumulations are coincident with areas of stagnant to slow-moving glacial ice flow (Schutt et.al, 2020). Ice flow measured by ANSMET indicate rates of 5 to 30 cm/yr in the slower moving areas (ANSMET, unpublished data) where abundant meteorites have been found. Over long

periods of time substantial deformation of an initial strewnfield extent can result. Surface exposure studies of moraines and bedrock in the Central Transantarctic Mountains are beginning to paint a picture of a relatively stable icesheet over several glacial cycles with higher ice surface thicknesses of 25-50 m higher prior to ~12,000 years, at the end of the Last Glacial Maximum and 50 to <100 m over the last 300,00-500,000 years. (Bader, et al., 2017, Kaplan et. al., 2019, Balter-Kennedy, 2020). Therefore, only small changes to ice velocities and dynamics are expected in most of the stranding sites mentioned in this study.

Strewnfield geometry can also change with meteorite type - irons, ordinary chondrites, carbonaceous chondrites, and achondrites all have different physical properties and will form strewnfields of distinct size and mass distribution. Such geometries are also dependent upon impact angle, and other physical parameters (e.g., Kress, et al., 2007). In addition, mineral assemblages, mineral compositions, magnetic susceptibility, terrestrial ages (if available), and/or NTL have all been used to help elucidate pairing relations. To further complicate interpretation, in dense collection areas like those searched in Antarctica, all members of a strewnfield may not have been recovered.

We examine potential pairing among the specimens from the four dense collection areas studied and compare their recovery mass and locations with those of some known pairing groups and strewnfields that include irons and stony irons, achondrites, ordinary (with E and R) chondrites, and carbonaceous chondrites (**Figure 6**; Supplementary Figures and **Tables S1 and S2**). In some cases unique meteorite types that are easy to justify as representing a strewnfield can be used to examine the scale and size of potential Antarctic strewnfields in general (e.g., distinct iron meteorites such as MET 00400 IIIAB or rare CMS 04061 pallasites or EET 87711 CR chondrite; **Table S2**) Such straightforward examples can then be applied to more difficult

cases such as pairing groups comprised of more common meteorite types or numerous members (some less straightforward exceptions might be the Larkman Nunatak shergottites, LEW angrites, or Almahata Sitta polymict breccia all of which have more than one lithology or multiple pairing groups within a dense collection area – special caution must be observed in interpretations in those cases). We then propose some pairing adjustments to reflect updated information available for the samples and a re-assessment of pairing in light of newer additional field seasons since the last assessment (Benoit et al. 2000).

Elephant Moraine Icefields

We recommend that pairing among the Elephant Moraine icefields L3 chondrites be revised substantially based upon our work, and propose new pairing groups.

Texas Bowl Icefield (L3.00)

Our results confirm the primitive nature of EET 90161 and are consistent with its classification of L3.00, along with EET 90066, 90261, and 90909 (**Table 1**). Although these chondrites and other low grade unequilibrated ordinary chondrites from EET exhibit textures of close-packed aggregate of chondrules in a dark matrix containing minor iron-nickel metal and troilite (e.g., Score and Lindstrom, 1992, 1994), these four samples have a distinctly higher σ-Cr_2O_3 than the other 3.00 samples from EET (see below and **Figure 1**), and exhibit a slightly higher range of Cr_2O_3 contents. These four samples are from a tight cluster of specimens within 1.5 kilometers each other (purple squares, **Figure 2**). The mass of the four Texas Bowl L3.00 specimens totals ~18 g; these mass and distance values are consistent with a small shower (**Figure 6**), such as Kosice (e.g., Borovicka et al., 2013).

Northern Ice Patch (L3.00)

EET 92100, is from the Northern Ice Patch, and is nearly 30 km from Texas Bowl group (**Figure 2,** purple square and only sample plotted in the northern ice patch). If these samples were part of a single strewnfield or shower, a 30 km extent would imply mass of ~ 100 kg, such as Pultusk or Weston (Lang and Kowalski, 1971; Schultz et al., 1972). The masses recovered from EET are not nearly this high, and suggest instead that EET 92100, with a mass of 3.4 g, is a single unpaired L3.00 fall.

Texas Bowl (L3.05)

EET 87735, 90080, 90519, and 90916 are all L3.05 chondrites, and this group (EET 87735) is likely a small shower (**Figure 6**). As noted above, these samples all exhibit textural and petrographic features of low grade UOC, such as close-packed aggregate of chondrules with matrix containing minor iron-nickel metal and troilite, but the Type II chondrule olivines exhibit slightly higher σ-Cr_2O_3 values, and variable Cr_2O_3 compared to the EET 90161 group of L3.00, and thus represent a distinct grouping (**Figure 2**, yellow pentagons).

Texas Bowl (L3.10)

EET 90628 is a lone L3.10 meteorite (**Figure 2**, green cross; **Figure 1**).

Meteorite City (L3.15)

The two L3.15 chondrites from Meteorite City, (EET 96015 and EET 96216; white diamonds) found ~0.4 kilometers apart, are paired together and are too distinct in their olivine Cr_2O_3 content to be paired with any other L3.x chondrites, whether from Meteorite City or Texas Bowl (**Figure 1**).

Elephant Moraine (L3.2)

EET 83274 is an L3.2 from the ice in close proximity to the Elephant Moraine that looks distinct from the other 4 L3 breccias that have been recovered in that area (**Figure 2**, black asterisk, **Figure 1**).

Meteorite City and Texas Bowl (>L3.2)

Four other L3s from EET – 90083, 90098, 90542, from Texas Bowl and EET 96160 from Meteorite City (**Figure 2**, blue star; **Figure 1**) - have very low Cr_2O_3 contents in olivine, and thus by this approach can only be stated as ≥L3.2. In these cases we have not suggested any change to the current classification.

Lewis Cliffs

We also recommend that pairing among the Lewis Cliffs L3s be revised substantially. All samples have texture and petrology expected for UOC such as abundant close packed chondrules of various type, as well as dark matrix with minor iron-nickel metal and troilite (e.g., Score and Lindstrom, 1988), but our olivine compositions exhibit distinct groupings, and we thus propose the following new pairing groups.

L3.00

LEW 86134 and LEW 87208, both identified here as L3.00, are likely too far apart – nearly 25 km – to be paired together, and thus are most likely two isolated finds (**Figure 3**, magenta squares). Continuous ice in the past may have allowed windblown separation of originally paired samples, but such a connection remains speculative.

L3.05

LEW 97202 is found close to LEW 87208 in the southernmost part of the region (**Figure 3**, blue hexagon), but their olivine compositions are distinctly different (**Figure 1**), and thus not paired based on our work.

L3.15

We have identified six L3.15's that are mostly on the northernmost ice tongue and could represent a shower (**Figure 3**, white diamonds), but could also be two groups (a group of 2 and a group of 4) since the two groups are ~ 25 km apart (LEW 87248 group; **Figure 6**). LEW 88462 has a lower Cr_2O_3 content and a higher σ-Cr_2O_3 value plotting higher than the trend, but in this case it is grouped with the 3.15 (**Figure 1**)

L3.2

Our analyses also reveal eight L3.2's that have olivine Cr_2O_3 contents between 0.1 and 0.15, and fall within 4 km of each other (**Figure 3**, black crosses; and LEW 86207 group; **Figure 6**). In addition, four samples were found to contain lower olivine Cr_2O_3 contents than expected for their petrologic type. LEW 86018 and LEW 86270 were previously classified as L3.1, but their olivine Cr_2O_3 contents are not high enough to support such a low petrologic type; they are here re-classified as L3.2. Similarly, LEW 86144 and LEW 86158 were previously classified as L3.0, but their olivine Cr_2O_3 contents are also not high enough to support such a low petrologic type; they are here re-classified as L3.2.

>L3.2

All the remaining LEW samples we examined have olivine Cr_2O_3 contents that are lower than those expected for 3.2, and thus we retain their classification (**Table 2**). In addition, the LEW DCA also contains 7 L breccias and these are also plotted in **Figure 3**, with all members

isolated finds and unpaired. In general, the LEW area contains a wide diversity of low petrologic type L chondrites, including three very primitive samples (**Figures 1 and 3**).

Grosvenor Mountains

The GRO samples were recovered over a very large geographic area – nearly 50 km in largest extent (**Figure 4a**). The GRO 95502 pairing group (Satterwhite and Lindstrom, 1997) is here reduced in number by two, with the suggestion that GRO 95558 be re-classified to L3.05 and GRO 95536 classification be retained as L3.3. The main group of GRO 95502 is re-classified as L3.2, consistent with the very similar Cr_2O_3 contents of its Type II chondrule olivine.

L3.05

GRO 06054 (**Figures 1 and 4**, purple star) was found in the more isolated region near Mauger Nunatak, and GRO 95558 (**Figures 1 and 4**, green star) was recovered from the Mt. Cecily-Mt. Raymond icefields, ~21.6 kilometers between their recovery locations (**Figure 4b**). The masses of the samples, 1318 g for GRO 06054 and 202 g for GRO 95558, might argue for a pairing. Ice flow and wind direction in the region are orthogonal to the line between the specimens, so neither are likely to have substantially contributed to their separation if they were paired specimens from a single fall. However, even though these samples are both L3.05, their mass–length traits fall below the main trend of strewnfields and other pairing groups (**Figure 6**), which might be more consistent with them being individual finds than paired stones (**Figure 1**). A close comparative analysis and terrestrial age dating of these samples would be appropriate and may increase the level of confidence in this pairing issue.

L3.10

GRO 03015 and 03061, on the other hand, were recovered near each other on the Otway Massif icefield, only 0.88 kilometers apart (**Figures 1 and 4**; purple triangles). The close proximity, similar petrography and textures, and similar olivine Cr_2O_3 content suggests that these L3.10 specimens are paired from a shower (**Figure 4**).

L3.2

Ten L chondrite GRO samples from the GRO group appear to be of petrologic type 3.2 (**Figures 1 and 4**, red diamonds). Nine specimens were recovered from the Mt. Cecily-Mt. Raymond bare ice areas (GRO 95502; Satterwhite and Lindstrom, 1997; **Figure 6 and Table S2**) and have been paired together since their original classification as L3.5 (suggested here to be L3.2 instead). A single specimen was found at the Mt. Bumstead Icefield, ~14.0 kilometers from the nearest Cecily-Raymond L3.2 (**Figures 1 and 4**; blue diamond). Neither ice flow nor wind direction would likely have contributed much to this physical separation; as with the L 3.05 specimens mentioned above, the possibility that the Mt. Bumstead specimen being paired with the Cecily-Raymond group cannot be ruled out, but seems unlikely.

>L3.2

One meteorite examined from the Cecily-Raymond icefield (GRO 95536; **Figure 4**, yellow pentagon) has the lowest olivine Cr_2O_3 content and thus we suggest retaining its current classification as an L3.3 (**Table 3 and Figure 4a, 4b**).

Meteorite Hills

In contrast to the EET and GRO meteorite recovery areas, The Meteorite Hills represent a fairly continuous and relatively small localized icefield. The meteorites from this site in our study are found within a relatively small area, and thus could represent a shower fall. H, L, and

L/LL UOC were identified here (e.g., Satterwhite and Allen, 2002; Satterwhite and Righter, 2010; Satterwhite and Lindstrom, 1998), and the textural and petrographic features within the L and L/LL are certainly permissive of large pairing groups, but the diversity of petrologic types suggests otherwise, as described below.

L/LL3.05

MET 00452 and 00526 were previously re-classified as L/LL3.05 (Satterwhite and Righter, 2010), and our work indicates that MET 00621 may be paired together as well (**Figures 1 and 5**; blue squares). MET 00452 and 00526 were found 0.2 kilometers from one another while MET 00621 was found ~4.5 kilometers from the other two. This makes three L/LL3.05 meteorites that are likely part of a small shower (**Figure 6**).

L3.10 and H3.10

There are five MET L3.10 specimens from the 1996 and 2001 field seasons, and three H3.10 from the 2000 field season (**Figures 1 and 5**; yellow diamonds and purple stars, respectively; Satterwhite and Lindstrom, 1998; Satterwhite and Righter, 2003); these represent two pairing groups (MET 96503 and MET 00506, respectively; **Figure 6**). The furthest any specimen of the L3.10 group was found apart from one other fragment was 7.9 kilometers. Two fragments, MET 00506 and MET 00552, of the H3.10 group were found 0.26 kilometers from each other while MET 00607 was found ~2.6 kilometers distant.

>L3.2

There are three MET samples that have olivine Cr_2O_3 contents <0.10 wt% and their classifications are thus unchanged; one of these samples, MET 00489, remains classified as L3.6 (**Figures 1 and 5**; cyan pentagon), while the other two MET 00570 and 01182, are H3.8

(**Figures 1 and 5**; red triangles) and may be paired with each other, having been found only 5.0 kilometers from one another (**Table 4 and Figure 5**).

Given the spatial distribution of these small showers and the setting at Meteorites Hills it is speculated that the meteorites have not travelled a great distance in the ice or moved significant distances while on the ice surface since they arrived.

Summary

Although the primary goal of this work was to identify primitive chondrites that may have been unrecognized in previous work, we have included a large number of samples from regions where pairing has not been re-assessed in decades and samples have been recovered over multiple and successive collection seasons. We have identified additional primitive members, and where possible updated or re-assessed pairing. Specifically, we have identified 23 additional primitive (3.10 or lower) ordinary chondrites that will be of interest to many meteoriticists who study origins and nebular processes. However, because the measurement of Cr_2O_3 in olivine is not especially sensitive to identification of petrologic type >3.2, we have not been able to fully update samples and pairings from every area. Detailed pairing assessments would benefit from cosmic ray exposure age dating; such studies would undoubtedly shed light on these groupings and thus be of some value in future work.

Acknowledgements

We thank Anne Peslier for assistance with the Cameca electron microprobe at NASA-JSC, and Jeff Grossman for sharing unpublished microprobe data for MET samples. All DigitalGlobe Worldview and Ikonos satellite imagery was acquired through Polar Geospatial Center. Support for this work provided by the Polar Geospatial Center under NSF-OPP awards 1043681 and 1559691).

References

Alexander, C. M., Newsome, S. D., Fogel, M. L., Nittler, L. R, Busemann, H., Cody, G. D., (2010) Deuterium enrichments in chondritic macromolecular material-Implications for the origin and evolution of organics, water and asteroids. Geochimica et Cosmochimica Acta 74, 4417-4437.

Bader, N., Licht, K., Kaplan, M., Kassab, C., Winckler, G. (2017) East Antarctic ice sheet stability recorded in a high-elevation ice-cored moraine. Quaternary Science Reviews. 159. 88-102. 10.1016/j.quascirev.2016.12.005.

Balter-Kennedy, A. and Bromley, G. and Balco, G. and Thomas, H. and Jackson, M. S. (2020) A 14.5-million-year record of East Antarctic Ice Sheet fluctuations from the central Transantarctic Mountains, constrained with cosmogenic He, ^{10}Be, ^{21}Ne, and ^{26}Al, The Cryosphere, 14, No.8, 2647-2672.

Benoit, P. H., Sears, D. W., Akridge, J. M., Bland, P. A., Berry, F. J., & Pillinger, C. T. (2000) The non-trivial problem of meteorite pairing. *Meteoritics & Planetary Science* 35, 393-417.

Benoit, P. H., Akridge, G. A., Ninagawa, K., Sears, D. W. G. (2002) Thermoluminescence sensitivity and thermal history of type 3 ordinary chondrites: Eleven new type 3.0-3.1 chondrites and possible explanations for differences among H, L, and LL chondrites. Meteoritics & Planetary Science 37, 793-805.

Bonal, L., Quirico, E., Flandinet, L., Montagnac, G. (2016) Thermal history of type 3 chondrites from the Antarctic meteorite collection determined by Raman spectroscopy of their polyaromatic carbonaceous matter. Geochimica et Cosmochimica Acta 189, 312-337.

Borovička, J., Tóth, J., Igaz, A., Spurný, P., Kalenda, P., Haloda, J., ... & Husárik, M. (2013) The Košice meteorite fall: Atmospheric trajectory, fragmentation, and orbit. Meteoritics & Planetary Science 48, 1757-1779.

Busemann, H., Alexander, C. M. O'D., Nittler, L. R. (2007) Characterization of insoluble organic matter in primitive meteorites by microRaman spectroscopy. Meteoritics & Planetary Science 42, 1387-1416.

Davidson, J., Nittler, L.R., Alexander, C.M., & Stroud, R.M. (2014) Petrography of very primitive CO3 chondrites: Dominion Range 08006, Miller Range 07687, and four others. In *Lunar and Planetary Science Conference* (No. 1777, p. 1384).

Doyle, P.M., Jogo, K., Nagashima, K., Krot, A. N., Wakita, S., Ciesla, F.J., Hutcheon, I.D., (2015) Early aqueous activity on the ordinary and carbonaceous chondrite parent bodies recorded by fayalite. Nature communications, 6.

Grossman, J.N., Brearley, A.J. (2005) The onset of metamorphism in ordinary and carbonaceous chondrites. Meteoritics & Planetary Science 40, 87-122.

Kaplan. M., Licht, K., Winkler, G., Kassab. C., Lamp, J., Schaefer, J., and Graly. J. (2019) Surface changes at the head of the Law Glacier and Interior EAIS during the last ~100, ~10,000, ~100,000, and ~0.5 million years, (Abstract), 4th Interdisciplinary Antarctic Earth Sciences Conference.

Kimura, M., Grossman, J.N., Weisberg, M.K. (2008) Fe-Ni metal in primitive chondrites: Indicators of classification and metamorphic conditions for ordinary and CO chondrites. Meteoritics & Planetary Science 43, 1161-1177.

Kress, M.E., Benedix, G.K., Schutt, J., & Harvey, R.P. (2007). An Unusual Strewn Field at the Otway Massif, Grosvenor Mountains, Antarctica. *Meteoritics and Planetary Science Supplement*, *42*, 5270.

Lang, B., & Kowalski, M. (1971). On the Possible Number of Mass Fragments From Pultusk Meteorite Shower, 1868. *Meteoritics*, *6*(3), 149-158.

Lauretta, D.S., Nagahara, H., Alexander, C.M.O'D. (2006) Petrology and origin of ferromagnesian silicate chondrules. Meteorites and early solar system II, 431-459.

Marvin, U.B. (1989) Meteorite distributions at the Allan Hills Main icefield and the pairing problem. *Smithsonian Contrib Earth Sci 28*, 113-119.

Mishra, R.K. and Goswami, J.N. (2014) Fe-Ni and Al-Mg isotope records in UOC chondrules: Plausible stellar source of 60Fe and other short-lived nuclides in the early Solar System. Geochimica et Cosmochimica Acta 132, 440-457.

Nittler, L.R., Alexander, C. M. O'D., Gallino, R., Hoppe, P., Nguyen, A. N., Stadermann, F. J., Zinner, E. K. (2008) Aluminum-, Calcium- and Titanium-rich Oxide Stardust in Ordinary Chondrite Meteorites. Ap. J. 682, 1450.

Satterwhite, C.E. and Lindstrom, M.M. (1997) Antarctic Meteorite Newsletter 20, no. 2, p. 10.

Satterwhite, C.E. and Lindstrom, M.M. (1998) Antarctic Meteorite Newsletter 21, no. 2, p. 17.

Satterwhite, C.E. and Righter, K. (2003) Antarctic Meteorite Newsletter 26, no. 1, p. 18.

Satterwhite, C.E. and Righter, K. (2010) Antarctic Meteorite Newsletter 33, no. 1, p. 3.

Schultz, L., Signer, P., Lorin, J.C., & Pellas, P. (1972) Complex irradiation history of the Weston chondrite. Earth and Planetary Science Letters 15, 403-410.

Schutt, J.W., Harvey, R.P., Kelleher, C. and Karner, J. (2020) The complex relationship between Antarctic meteorite concentrations and ice velocity (Abstract), 51st Lunar and planetary Science Conference.

Score, R. and Lindstrom, M.M. (1994) Antarctic Meteorite Newsletter 17, no. 3.

Score, R. and Lindstrom, M.M. (1992) Antarctic Meteorite Newsletter 15, no. 2, p. 26.

Score, R. and Lindstrom, M.M. (1988) Antarctic Meteorite Newsletter 11, no. 1, 13-14.

Scott, E.R.D. (1984) Pairing of meteorites found in Victoria Land, Antarctica. Memoirs of National Institute of Polar Research. Special issue 35, 102-125.

Sears D.W.G., Grossman J.N., Melcher C.L., Ross L.M., and Mills A.A. (1980) Measuring metamorphic history of unequilibrated ordinary chondrites. *Nature* 287, 791–795.

Sears, D.W.G., Hasan, F.A., Batchelor, J.D., Lu, J. (1991) Chemical and physical studies of type 3 chondrites. XI-Metamorphism, pairing, and brecciation of ordinary chondrites. Proceedings Lunar and Planetary Science Conference 21, 493-512.

Simon, S.B., & Grossman, L. (2015) Refractory inclusions in the pristine carbonaceous chondrites DOM 08004 and DOM 08006. *Meteoritics & Planetary Science 50*, 1032-1049.

Telus, M., Huss, G. R., Nagashima, K., Ogliore, R. C., & Tachibana, S. (2018) In situ ^{60}Fe-^{60}Ni Systematics of Chondrules from Unequilibrated Ordinary Chondrites. Geochimica et Cosmochimica Acta 221, 342-357.

Van Schmus W.R. and Wood J.A. (1967) A chemical-petrologic classification for the chondritic meteorites. *Geochimica et Cosmochimica Acta* 31, 747–765.

Wasson, J.T., Krot, A.N., Lee, M.S., Rubin, A.E. (1995) Compound chondrules. Geochimica et Cosmochimica Acta 59, 1847-1869.

Wasson, J.T. (1990) Ungrouped iron meteorites in Antarctica: Origin of anomalously high abundance. *Science* 249, 900-902.

Welten, K.C., Lindner, L., Alderliesten, C., & Van der Borg, K. (1999) Terrestrial ages of ordinary chondrites from the Lewis Cliff stranding area, East Antarctica. *Meteoritics & Planetary Science* 34, 559-569.

Welten, K.C., Nishiizumi, K., Masarik, J., Caffee, M.W., Jull, A.J.T., Klandrud, S.E., & Wieler, R. (2001) Cosmic-ray exposure history of two Frontier Mountain H-chondrite showers from spallation and neutron-capture products. *Meteoritics & Planetary Science* 36, 301-317.

Zega, T.J., Nittler, L.R., Gyngard, F., Alexander, C.M.O'D., Stroud, R.M., Zinner, E.K. (2014) A transmission electron microscopy study of presolar spinel. Geochimica et Cosmochimica Acta 124, 152-169.

Figure Captions

Figure 1: Summary of Cr_2O_3 analyses for olivines in Type II chondrules in unequilibrated ordinary chondrites from the four dense collection areas considered in this work: EET, LEW, MET and GRO. Petrologic type boundary curves and labels are from Grossman and Brearley (2005). Individual samples labels and Cr_2O_3 and σCr_2O_3 values are as specified in Tables 1 to 4. The symbols in each plot correspond to the symbols in each DCA map – Figures 2, 3, 4, and 5.

Figure 2: EET region showing the locations of L3 chondrites and newly recognized primitive chondrites reported in Table 1, as well as the subfields Northern Icefield, Texas Bowl, Meteorite City, and Elephant Moraine. EET 92100 in the Northern Icefield is L3.00. Texas Bowl samples EET 90066, 90161, 90261, and 90909 are L3.00. Texas Bowl samples EET 87735, 90080, 90519, 90916 are L3.05. EET 90628 is L3.10, and EET 90083, 90098, and 90542 are L3.5, L3.7, and L3.8, respectively. Meteorite City samples EET 96015, and 96216 are L3.15 and EET 96160 is L3.6. Finally, Elephant Moraine sample EET 83274 is L3.2. **Satellite Image Acknowledgement**: Figure 2 – Landsat Image - Landsat Image Mosaic of Antarctica (LIMA) Project.

Figure 3a and Figure 3b: Figure 3a is a mosaic image of the Lewis Cliff Icefields showing the locations of all L3 chondrites. Figure 3b shows the locations of the newly recognized primitive chondrites from the Lewis Cliff Ice Tongue as reported in Table 2. LEW 86134 and 87208 are L3.00. LEW 97202 is L3.05. LEW 87248, 87284, 88254, 85434, 85437, and 88462 are all L3.15. LEW 86207, 86102, 88634, 88520, 86018, 86144, 86158, and 86270 are all L3.2. Other samples are >L3.2, as indicated in Table 2. **Satellite Image Acknowledgement**: Figure 3a – ASTER Image - NASA/GSFC/METI/ERSDAC/JAROS, and U.S./Japan ASTER Science Team

and Worldview 2 image – 27 January 2014 (© 2014 DigitalGlobe Inc.). Geospatial support for this work provided by the Polar Geospatial Center under NSF-OPP awards 1043681 and 1559691. Figure 3b - ASTER Image - NASA/GSFC/METI/ERSDAC/JAROS, and U.S./Japan ASTER Science Team.

Figure 4a and Figure 4b: GRO region (left) showing the locations of L3.x chondrites and the newly recognized primitive chondrites reported in Table 3, and the subfields Otway Massif, Mt. Bumstead, Mt. Cecily-Mt. Raymond, and Block Peak-Mauger-Mt. Block. Right side map shows an enlarged portion of the Mt. Cecily-Mt. Raymond region. GRO 95558 (Cecily-Raymond) and GRO 06054 (Block Peak-Mauger-Mt. Block) are L3.05. GRO 03015 and 03061 (both Otway Massif) are L3.10. GRO 95502, 95504, 95512, 95539, 95542, 95544, 95545, 95546, 95550 (all Cecily-Raymond) and 95505 (Mt. Bumstead) are all 3.2, and GRO 95536 is L3.3 (Cecily-Raymond). **Satellite Image Acknowledgement**: Figure 4a – MODIS RapidFire Hole Filler V1.4. MODIS South Pole Mosaic created by the Polar Geospatial Center. Support for this work provided by the Polar Geospatial Center under NSF-OPP awards 1043681 and 1559691). Figure 4b – Worldview 1 image – 10 February 2010 (© 2010 DigitalGlobe Inc.).

Figure 5: MET region showing the newly recognized primitive chondrites reported in Table 4. MET 00452, 00526, and 00621 are all L/LL3.05; MET 96503, 96515, 01051, 01056, and 01057 are L3.10; MET 00506, 00552, and 00607 are H3.10. MET 00489 is L3.6, and MET 00570 and 01182 are H3.8. **Satellite Image Acknowledgement**: Landsat Image - Landsat Image Mosaic of Antarctica (LIMA) Project.

Figure 6: Mass and approximate length of known strewnfields (open symbols) for (A) irons and stony irons (Campo del Cielo; Canyon Diablo; Gibeon, Henbury, Vaca Muerta, Lowicz), (B)

achondrites (Camel Donga, Johnstown, Stannern, Puerto Lapice, Tirhert, and Almahata Sitta), (C) ordinary chondrites (S1=SaU 001, W=Weston, Tenham, Villalbeto de la Pena, SS=St. Severin, Stubenberg, Pu=Pultusk, Modoc, Mocs, L'Aigle, Ku=Kunashak, Kr=Krymka, Kosice, Kn=Knyahinya, Jilin, Hs=Homestead, Chelyabinsk, Br=Bruderheim, Ba=Barwell, PF=Park Forest, Plainview), and (D) carbonaceous chondrites (Allende, DaG 749, Kainsasz, Sutters Mill, Orgueil, Moss, Murchison, Tagish Lake, and Aguas Zarcas). All data were assembled from sources as described in the Supplementary information Table S1. These well documented strewnfields are compared to some ANSMET pairing groups (grey symbols; supplementary information, Table S2 and Figures S1-S14), as well as 8 potential pairing groups discussed in this work (solid symbols; EET, LEW, GRO, and MET areas). All data are summarized and described in **Supplementary Tables and Figures**.

Table 1: Olivine analyses from UOC from Elephant Moraine Icefield (EET); meteorites part of a pairing group are separated by a blank row

sample	Mass (g)	TS#	SiO_2	Al_2O_3	Cr_2O_3	FeO	MnO	NiO	MgO	CaO	Total	σ Cr_2O_3	n	subfield	current	new data	revised
EET 83274	82.70	7	38.88	0.04	0.188	18.23	-	0.03	42.47	0.13	99.97	0.085	16	Elephant Moraine	L3.6	L3.2	L3.2
EET 90066	9.764	3	39.87	0.09	0.411	13.76	-	0.041	45.99	0.12	100.28	0.098	28	Texas Bowl	L3.3	L3.00	L3.00
EET 90161	9.708	6	40.26	0.07	0.428	13.90	-	0.080	45.42	0.12	100.28	0.086	15	Texas Bowl	L3.0	L3.00	L3.00
EET 90261	6.640	3	40.80	0.04	0.414	11.77	-	0.029	47.67	0.11	100.83	0.110	22	Texas Bowl	L3.4	L3.00	L3.00
EET 90909	6.428	3	39.65	0.057	0.420	14.19	-	0.025	45.94	0.12	100.40	0.120	36	Texas Bowl	L3.6	L3.00	L3.00
EET 87735	4.160	4	39.27	0.03	0.409	15.50	-	0.047	44.46	0.13	99.84	0.138	18	Texas Bowl	L3.4	L3.05	L3.05
EET 90080	4.104	3	39.09	0.04	0.438	15.78	0.36	0.031	44.16	0.14	100.03	0.136	34	Texas Bowl	L3.4	L3.05	L3.05
EET 90519	5.214	4	39.79	0.05	0.430	14.00	-	0.034	45.82	0.12	100.24	0.140	36	Texas Bowl	L3.6	L3.05	L3.05
EET 90916	4.645	3	39.55	0.02	0.451	14.48	-	0.08	45.53	0.12	100.22	0.139	38	Texas Bowl	L3.6	L3.05	L3.05
EET 90628	23.056	6	39.26	0.056	0.350	15.15	-	0.035	44.79	0.11	99.75	0.180	28	Texas Bowl	L3.4	L3.10	L3.10
EET 90083	3.601	3	38.16	0.03	0.083	22.49	-	0.042	39.14	0.044	99.99	0.110	24	Texas Bowl	L3.5	>L3.2	L3.5
EET 90098	4.717	3	37.81	0.02	0.059	23.01	-	0.02	38.61	0.06	99.59	0.096	29	Texas Bowl	L3.7	>L3.2	L3.7
EET 90542	4.968	3	38.72	0.03	0.052	19.21	-	0.02	41.86	0.07	99.97	0.047	31	Texas Bowl	L3.8	>L3.2	L3.8
EET 92100	3.383	4	39.85	0.13	0.430	13.79	-	0.03	45.87	0.11	100.21	0.080	31	Northern	L3.4	L3.00	L3.00
EET 96015	0.521	4	38.53	0.01	0.246	19.68	-	0.03	41.35	0.13	99.96	0.165	23	Meteorite City	L3.4	L3.15	L3.15
EET 96216	0.868	3	38.53	0.02	0.179	19.49	-	0.05	41.60	0.07	99.93	0.193	25	Meteorite City	L3.8	L3.15	L3.15
EET 96160	0.882	3	38.86	0.05	0.055	17.79	-	0.09	43.05	0.09	99.99	0.073	25	Meteorite City	L3.6	>L3.2	L3.6

TS# = thin section number studied; n = number of olivine analyses per section; "-" signifies not analyzed

Table 2: Olivine analyses from UOC from Lewis Cliffs Icefield (LEW) ; meteorites part of a pairing group are separated by a blank row (*=southernmost grouping)

Sample	Mass (g)	TS#	SiO_2	TiO_2	Al_2O_3	Cr_2O_3	FeO	MnO	NiO	MgO	CaO	Total	σ Cr_2O_3	n	current	New data	revised
LEW 86134	28.935	4	38.19	-	-	0.410	14.61	0.38	-	46.06	0.13	99.78	0.082	25	L3.0	L3.00	L3.00
LEW 87208*	34.460	12	38.55	-	0.02	0.38	13.9	0.36	-	46	0.12	99.33	0.095	18	L3.4	L3.00	L3.00
LEW 97202*	117.596	5	38.28	-	0.03	0.44	15.55	0.42	-	44.31	0.14	99.17	0.143	28	L3.4	L3.05	L3.05
LEW 87248*	13.847	2	39.31	-	0.08	0.27	15.44	0.36	-	43.79	0.16	99.41	0.16	16	L3.5	L3.15	L3.15
LEW 87284*	38.600	3	38.85	-	0.02	0.28	17.46	0.36	-	42.54	0.13	99.64	0.15	32	L3.5	L3.15	L3.15
LEW 88254	13.487	3	39.57	-	0.02	0.24	14.35	0.38	-	45.06	0.12	99.74	0.08	33	L3.4	L3.15	L3.15
LEW 85434	19.358	5	38.67	-	0.05	0.22	18.23	0.40	-	41.95	0.14	99.65	0.110	30	L3.4	L3.15	L3.15
LEW 85437	9.373	4	39.36	-	0.02	0.25	15.71	0.42	-	43.43	0.11	99.30	0.180	21	L3.4	L3.15	L3.15
LEW 88462	8.064	3	39.57	-	0.02	0.10	17.83	0.44	-	42.90	0.07	100.92	0.25	27	L3.7	L3.15	L3.15
LEW 86207	17.732	7	39.15	0.01	0.02	0.144	16.03	0.33	0.02	43.92	0.07	99.69	0.118	18	L3.2	L3.2	L3.2
LEW 86102	21.753	8	39.47	b.d.l.	0.03	0.170	15.05	0.39	0.03	42.80	0.09	98.04	0.067	23	L3.4	L3.2	L3.2
LEW 88634	7.712	7	37.96	-	0.04	0.15	16.93	0.37	-	43.47	0.11	99.03	0.066	30	L3.4	L3.2	L3.2
LEW 88520	3.127	3	39.15	-	0.01	0.15	18.78	0.40	-	41.67	0.10	100.25	0.11	32	L3.5	L3.2	L3.2
LEW 86018	502.0	25	39.10	b.d.l.	0.02	0.142	15.48	0.38	0.02	44.92	0.10	100.17	0.067	34	L3.1	L3.2	L3.2
LEW 86144	11.056	8	37.53	-	-	0.088	17.52	0.37	-	43.51	0.20	99.22	0.057	25	L3.0	L3.2	L3.2
LEW 86158	8.593	6	38.28	-	-	0.100	18.24	0.41	-	42.60	0.10	99.73	0.072	25	L3.0	L3.2	L3.2
LEW 86270	4.230	3	38.90	0.01	0.04	0.132	17.02	0.34	0.03	43.20	0.11	99.77	0.073	30	L3.1	L3.2	L3.2
LEW 85401	3.940	3	38.92	-	0.03	0.10	16.82	0.33	-	43.25	0.11	99.57	0.060	31	L3.3	≥L3.2	L3.3
LEW 86127	11.938	6	39.67	0.02	0.09	0.114	15.11	0.37	0.02	44.41	0.12	99.90	0.071	21	L3.3	≥L3.2	L3.3
LEW 88033	1.930	3	39.66	-	0.03	0.09	18.46	0.41	-	42.62	0.11	101.38	0.05	26	L3.3	≥L3.2	L3.3
LEW 85339	28.776	9	39.08	-	0.03	0.073	17.13	-	0.04	43.58	0.08	100.01	0.119	38	L3.4	≥L3.2	L3.4

LEW 86246	2.315	3	38.26	0.01	0.07	0.045	20.70	0.41	0.06	40.15	0.10	99.80	0.037	19	L3.4	≥L3.2	L3.4
LEW 86367	10.525	4	38.97	0.02	0.08	0.070	16.50	0.41	0.02	42.36	0.16	98.59	0.037	21	L3.4	≥L3.2	L3.4
LEW 86505	43.935	8	38.60	0.01	0.02	0.061	18.31	0.35	0.02	42.58	0.05	99.99	0.106	34	L3.4	≥L3.2	L3.4
LEW 88175	111.301	3	36.78	-	0.19	0.057	21.58	0.4	-	39.34	0.06	98.41	0.07	30	L3.4	≥L3.2	L3.4
LEW 88261	17.550	3	39.40	-	0.04	0.086	17.21	0.33	-	42.44	0.10	99.62	0.15	30	L3.4	≥L3.2	L3.4
LEW 88452	13.352	3	38.35	-	0.01	0.11	16.28	0.37	-	43.68	0.11	98.91	0.068	34	L3.4	≥L3.2	L3.4
LEW 86105	6.392	-	-	-	-	-	-	-	-	-	-	-	-	-	L3.4	-	L3.4
LEW 86213	27.883	-	-	-	-	-	-	-	-	-	-	-	-	-	L3.4	-	L3.4
LEW 86408	1.445	3	38.55	0.01	0.04	0.097	18.10	0.39	0.02	42.69	0.12	100.02	0.060	27	L3.5	≥L3.2	L3.5
LEW 86417	1.556	3	38.49	0.01	0.01	0.077	18.24	0.42	0.03	42.67	0.10	100.04	0.036	35	L3.5	≥L3.2	L3.5
LEW 86436	3.865	3	38.78	b.d.l	0.03	0.040	16.56	0.33	0.02	44.14	0.06	99.96	0.029	35	L3.5	≥L3.2	L3.5
LEW 86495	2.450	3	39.19	-	0.02	0.04	16.44	0.45	-	43.92	0.07	100.13	0.04	28	L3.5	≥L3.2	L3.5
LEW 88286	3.899	3	38.97	-	0.04	0.10	17.03	0.39	-	43.13	0.10	99.76	0.07	33	L3.5	≥L3.2	L3.5
LEW 88617	3.150	3	39.01	-	0.02	0.06	17.23	0.40	-	42.81	0.08	99.61	0.07	34	L3.5	≥L3.2	L3.5
LEW 88632	10.250	3	38.40	-	0.03	0.08	19.66	0.43	-	41.13	0.10	99.82	0.041	31	L3.5	≥L3.2	L3.5
LEW 88644	15.859	3	38.34	-	0.17	0.06	18.87	0.35	-	42.09	0.07	99.94	0.052	36	L3.5	≥L3.2	L3.5
LEW 85396	60.247	5	38.99	-	0.14	0.09	16.48	0.32	-	43.73	0.11	99.88	0.201	36	L3.6	≥L3.2	L3.6
LEW 85452	9.240	4	39.40	-	0.03	0.07	15.46	0.35	-	44.54	0.10	99.95	0.056	27	L3.6	≥L3.2	L3.6
LEW 86347	3.113	3	38.40	0.02	0.02	0.030	17.34	0.44	0.01	42.09	0.06	98.41	0.028	26	L3.6	≥L3.2	L3.6
LEW 88146	4.976	3	38.40	-	0.05	0.05	19.55	0.33	-	41.44	0.11	99.93	0.050	31	L3.6	≥L3.2	L3.6
LEW 88263	8.772	3	38.71	-	0.03	0.05	21.63	0.40	-	39.51	0.12	100.45	0.03	33	L3.7	≥L3.2	L3.7
LEW 88328	43.147	3	40.40	-	0.03	0.06	14.23	0.33	-	45.77	0.11	100.96	0.07	27	L3.7	≥L3.2	L3.7
LEW 88594	5.401	3	38.26	-	0.05	0.06	23.11	0.46	-	38.43	0.04	100.40	0.13	33	L3.7	≥L3.2	L3.7
LEW 88621	7.507	3	39.47	-	0.02	0.06	18.35	0.46	-	42.67	0.06	101.11	0.11	37	L3.7	≥L3.2	L3.7
LEW 88696	6.034	4	39.29	-	0.04	0.06	19.87	0.48	-	41.30	0.09	101.13	0.07	37	L3.7	≥L3.2	L3.7
LEW 93891	25.470	3	39.82	-	0.22	0.04	17.05	0.43	-	43.47	0.07	101.09	0.04	37	L3.7	≥L3.2	L3.7
LEW 97216*	22.995	4	38.97	-	0.07	0.08	18.91	0.41	-	41.92	0.07	100.43	0.10	18	L3.7	≥L3.2	L3.7

LEW 88467	6.610	3	40.28	-	0.05	0.05	14.39	0.24	-	45.69	0.12	100.81	0.03	30	L3.8	≥L3.2	L3.8
LEW 87093	7.047		-	-	-	-	-	-	-	-	-	-	-	-	L3.8	-	L3.8
LEW 86021	325.800	6	39.02	-	0.03	0.04	17.15	0.39	-	43.22	0.08	99.93	0.040	35	L3.5-3.9	≥L3.2	L3.5-3.9
LEW 86307	4.897	3	38.52	0.01	0.05	0.080	18.91	0.45	0.01	40.15	0.10	98.29	0.057	26	L3.3-3.5	≥L3.2	L3.3-3.5
LEW 85420	12.447	-	-	-	-	-	-	-	-	-	-	-	-	-	L3-6	-	L3-6
LEW 86022	351.700	-	-	-	-	-	-	-	-	-	-	-	-	-	L3.2-3.5	-	L3.2-3.5
LEW 86549	50.140	-	-	-	-	-	-	-	-	-	-	-	-	-	L3.0-3.7	-	L3.0-3.7
LEW 88549	4.909	-	-	-	-	-	-	-	-	-	-	-	-	-	L3.0-3.7	-	L3.0-3.7
LEW 97221*	47.963	-	-	-	-	-	-	-	-	-	-	-	-	-	L3-6	-	L3-6

TS# = thin section number studied; n = number of olivine analyses per section; "-" signifies not analyzed; b.d.l. = below detection limits

Table 3: Olivine analyses from UOC from Grosvenor Mountains (GRO); meteorites part of a pairing group are separated by a blank row

Sample	Mass (g)	TS#	SiO_2	TiO_2	Al_2O_3	Cr_2O_3	FeO	MnO	NiO	MgO	CaO	Total	σ Cr_2O_3	n	Current	New data	Revised
GRO 95558	202.386	5	38.24	0.01	0.02	0.460	17.23	0.39	0.04	43.18	0.13	99.70	0.147	33	L3.5	L3.05	L3.05
GRO 06054	1319.400	6	38.94	0.01	0.02	0.417	15.48	0.38	0.03	44.36	0.11	99.74	0.167	32	L3.6	L3.05	L3.05
GRO 03015	480.000	4	39.02	0.01	0.02	0.323	15.07	0.38	0.03	44.70	0.11	99.67	0.098	32	L3.6	L3.10	L3.10
GRO 03061	455.000	4	38.61	0.01	0.03	0.328	17.35	0.40	0.06	42.89	0.13	99.81	0.153	37	L3.6	L3.10	L3.10
GRO 95502	5362.700	5	38.96	-	0.04	0.112	17.32	0.38	-	43.46	0.12	100.38	0.049	35	L3.2	L3.2	L3.2
GRO 95504	4018.300	6	39.15	-	0.03	0.093	17.18	0.37	-	43.70	0.12	100.64	0.068	38	L3.5	L3.2	L3.2
GRO 95505	2031.000	14	39.12	-	0.03	0.116	16.95	0.36	-	43.52	0.10	100.19	0.066	35	L3.4	L3.2	L3.2
GRO 95512	840.400	6	38.91	-	0.02	0.128	17.84	0.38	-	42.91	0.13	100.32	0.064	36	L3.5	L3.2	L3.2
GRO 95539	269.800	6	37.99	-	0.04	0.126	20.05	0.41	-	40.81	0.13	99.55	0.063	30	L3.1	L3.2	L3.2
GRO 95542	276.700	5	38.66	-	0.02	0.105	19.48	0.41	-	41.68	0.12	100.47	0.072	35	L3.5	L3.2	L3.2
GRO 95545	142.051	7	38.49	0.01	0.02	0.111	17.04	0.40	0.02	43.77	0.12	99.98	0.087	36	L3.5	L3.2	L3.2
GRO 95544	626.000	17	39.27	b.d.l.	0.02	0.124	14.46	0.35	0.02	45.73	0.10	100.08	0.067	35	L3.2	L3.2	L3.2
GRO 95550	169.955	5	38.41	0.01	0.02	0.088	17.19	0.41	0.03	43.60	0.12	99.88	0.054	39	L3.5	L3.2	L3.2
GRO 95546	200.840	5	38.58	0.04	0.02	0.054	17.70	0.48	0.05	43.20	0.04	100.16	0.153	26	L3.8	L3.2	L3.2
GRO 95536	331.200	11	39.15	-	0.02	0.052	17.22	0.41	-	43.31	0.05	100.20	0.046	38	L3.3	>L3.2	L3.3

TS# = thin section number studied; n = number of olivine analyses per section; "-" signifies not analyzed; b.d.l. = below detection limits

Table 4: Olivine analyses from UOC from Meteorite Hills (MET); meteorites part of a pairing group are separated by a blank row

Sample	Mass (g)	TS#	SiO_2	TiO_2	Al_2O_3	Cr_2O_3	FeO	MnO	NiO	MgO	CaO	σ Cr_2O_3	Total	n	current	revised
MET 00452	774.900	15	38.99	0.01	0.04	0.44	17.52	0.47	0.09	42.17	0.19	0.17	99.92	81	L/LL 3.05	no change
MET 00526	208.200	8	39.53	0.01	0.02	0.48	13.36	0.5	-	44.94	0.17	0.16	99.01	42	L/LL 3.05	no change
MET 00621	88.835	5	38.54	-	0.03	0.49	13.98	0.35	-	45.88	0.13	0.257	99.39	28	L3.6	L/LL 3.05
MET 96503	404.000	5	38.79	0.02	0.03	0.32	13.99	0.53	-	43.98	0.17	0.22	97.83	37	L3.1	L3.10
MET 96515	308.700	5	39.07	0.01	0.03	0.29	18.49	0.44	0.02	42.27	0.14	0.14	100.76	44	L3.5	L3.10
MET 01051	621.100	5	38.97	0.01	0.02	0.29	17.22	0.4	0.03	43.03	0.16	0.15	100.13	44	L3.6	L3.10
MET 01056	397.100	5	38.72	0.01	0.02	0.3	18.96	0.45	0.03	41.31	0.16	0.21	99.96	45	L3.6	L3.10
MET 01057	189.290	5	39.35	0.01	0.03	0.41	15.25	0.4	0.02	44.25	0.15	0.22	99.87	45	L3.6	L3.10
MET 00506	301.100	19	38.92	-	0.01	0.40	14.84	0.37	-	44.91	0.11	0.297	99.57	37	H3.4	H3.10
MET 00552	97.300	7	38.9	0.01	0.01	0.33	17.59	0.43	0.02	42.43	0.15	0.16	99.87	41	H3.4	H3.10
MET 00607	76.550	13	38.68	-	0.01	0.39	15.22	0.38	-	44.63	0.12	0.194	99.42	36	H3.4	H3.10
MET 00489	232.000	6	38.27	0.02	0.04	0.09	20.14	0.44	0.03	40.94	0.07	0.135	100.03	27	L3.6	>L3.2
MET 00570	157.015	5	38.51	0.03	0.09	0.03	18.18	0.47	0.12	41.43	0.52	0.108	99.39	30	H3.8	>H3.2
MET 01182	69.860	6	36.57	-	0.02	0.06	26.10	0.46	-	36.16	0.15	0.080	99.52	16	H3.8	>H3.2

TS# = thin section number studied; n = number of olivine analyses per section; "-" signifies not analyzed

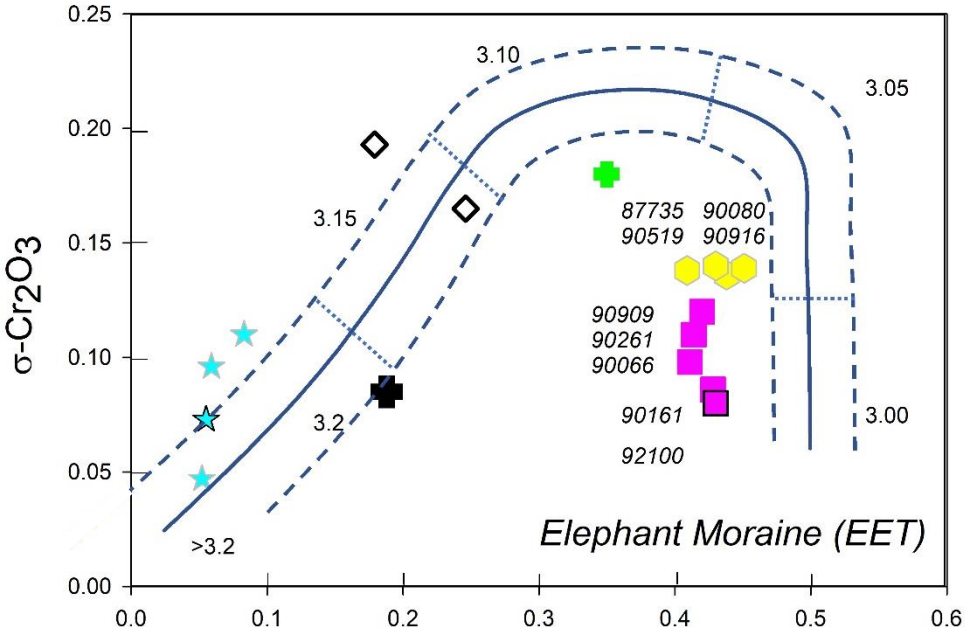
σ-Cr2O3
3.10
3.05
3.15
3.2
3.00
>3.2
87735 90080
90519 90916
90909
90261
90066
90161
92100
Elephant Moraine (EET)

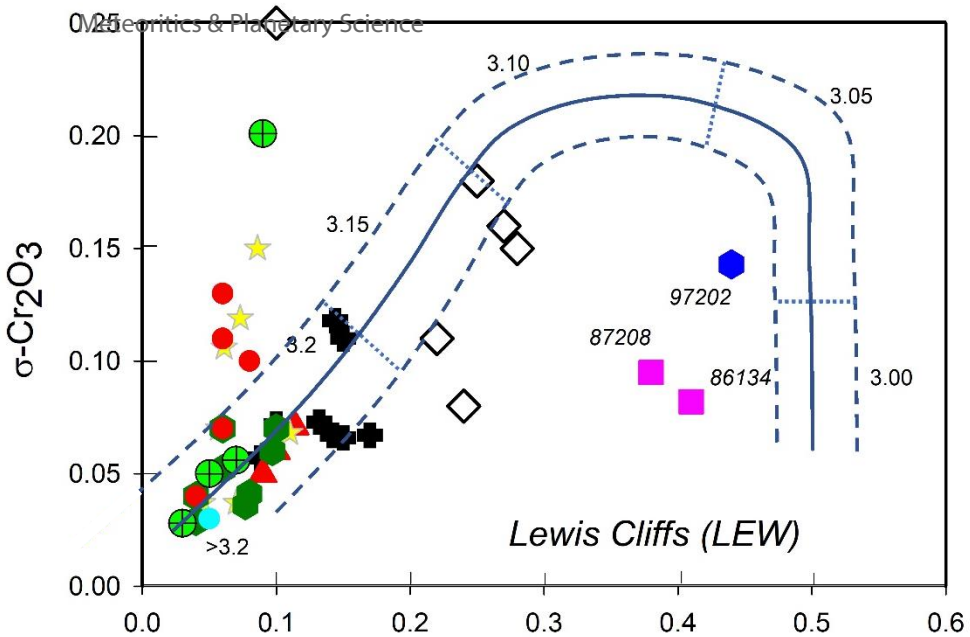
σ-Cr2O3
3.10
3.05
3.15
3.2
3.00
>3.2
97202
87208
86134
Lewis Cliffs (LEW)

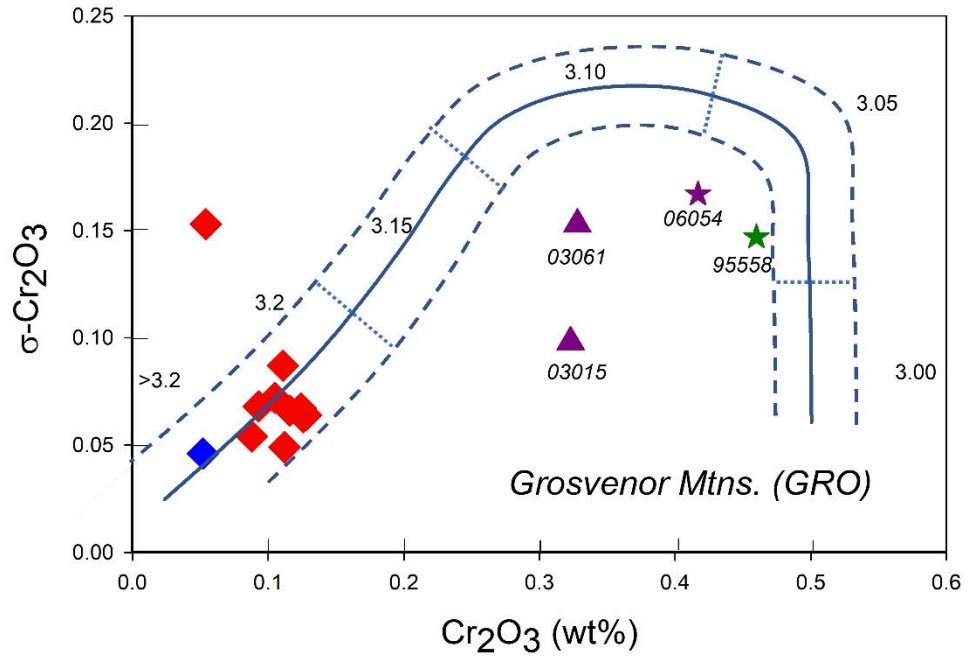
σ-Cr2O3
3.10
3.05
3.15
3.2
3.00
>3.2
06054
03061
95558
03015
Grosvenor Mtns. (GRO)
Cr2O3 (wt%)

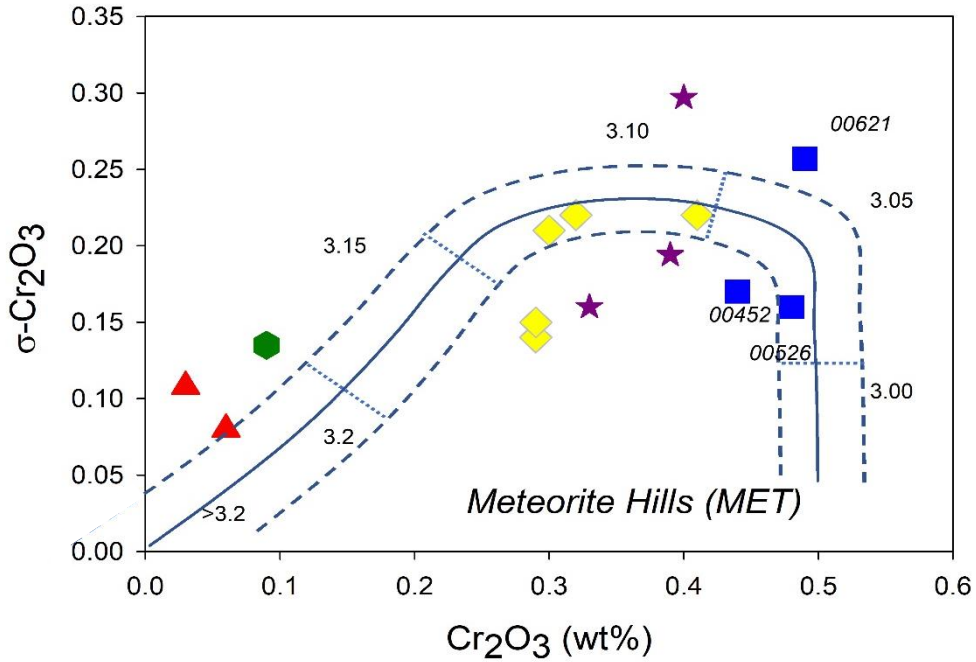
σ-Cr2O3
3.10
3.05
3.15
3.2
3.00
>3.2
00621
00452
00526
Meteorite Hills (MET)
Cr2O3 (wt%)

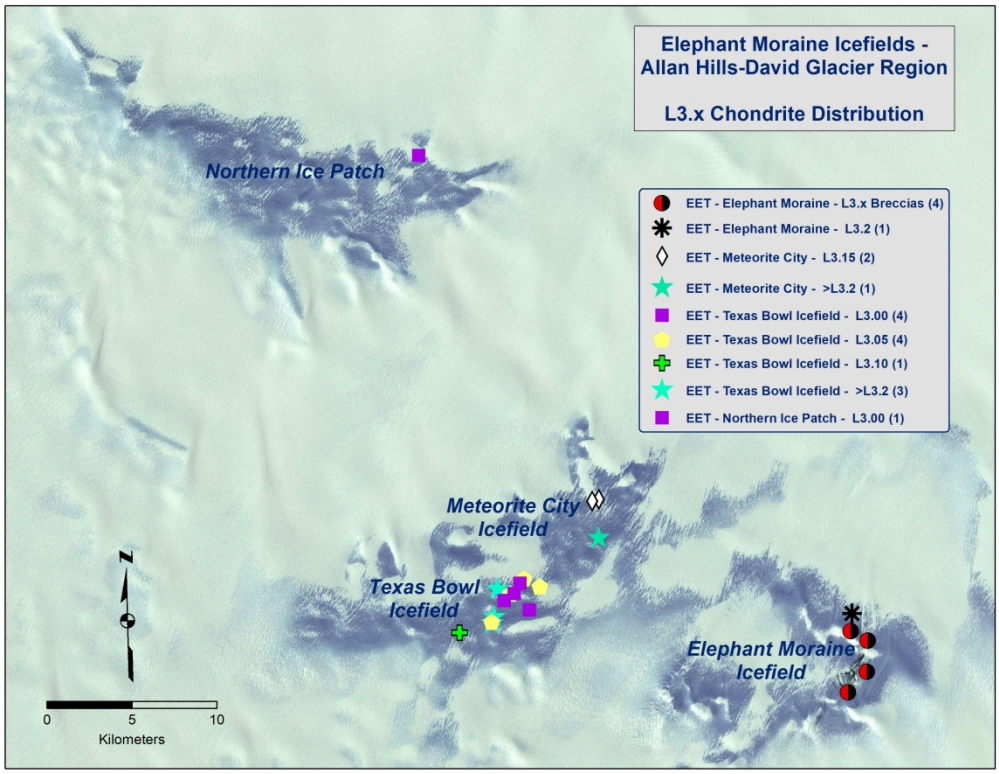

Figure 2

279x215mm (300 x 300 DPI)

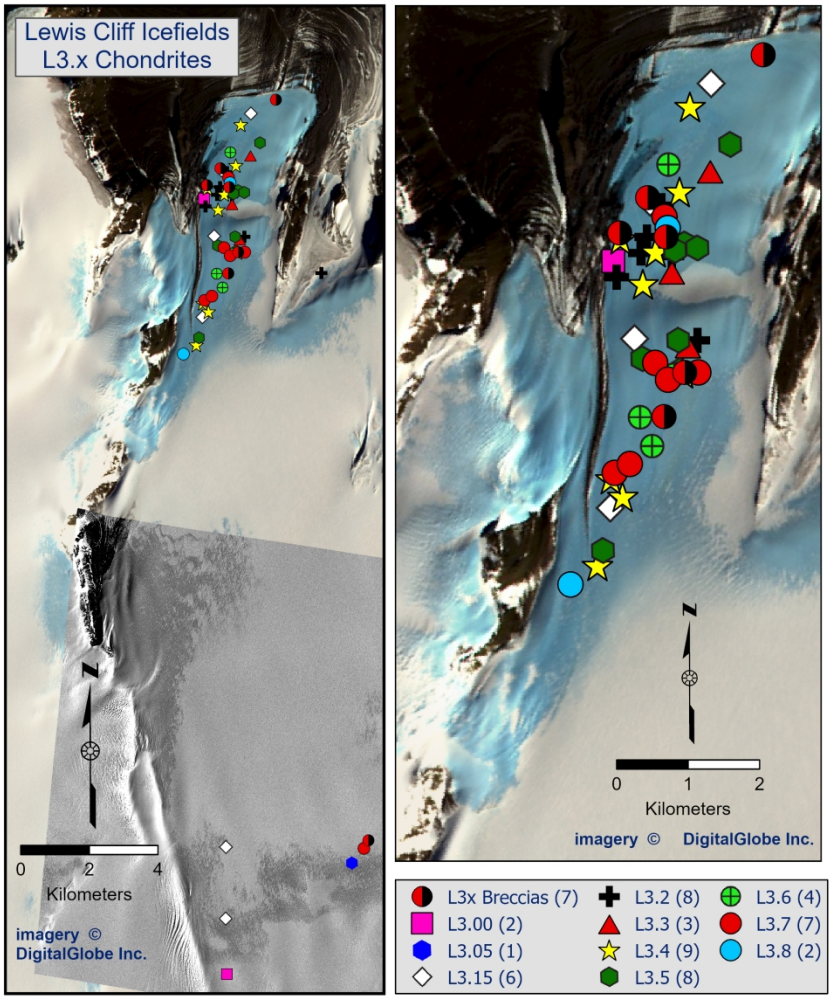

Figure 3

548x710mm (118 x 118 DPI)

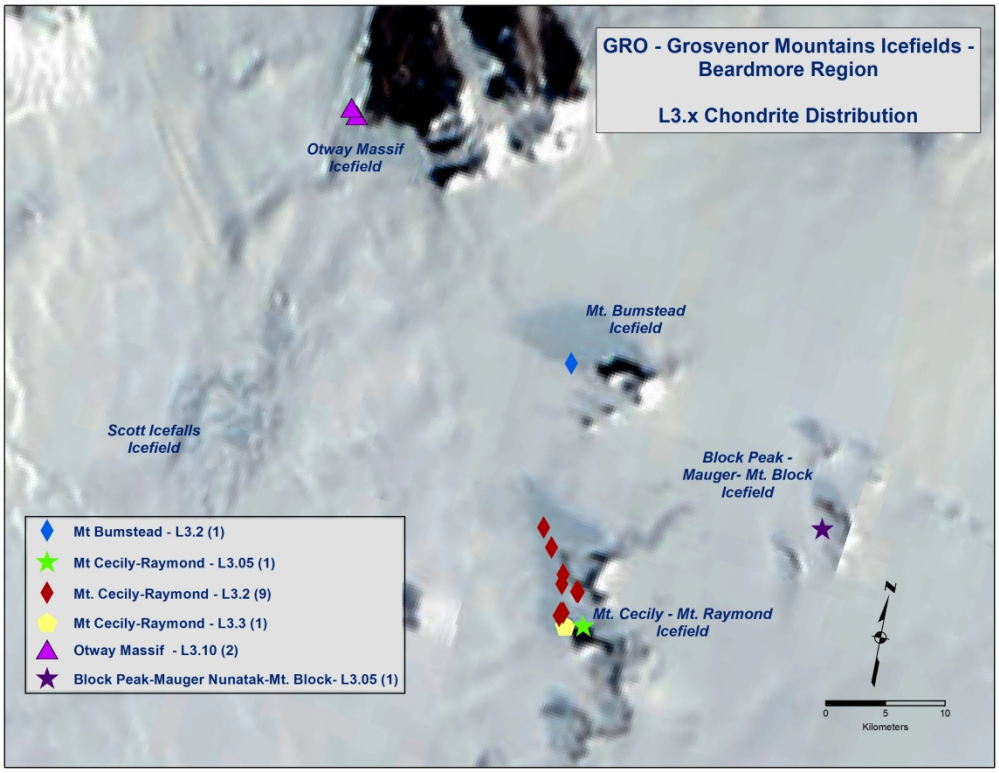

Figure 4a

279x215mm (300 x 300 DPI)

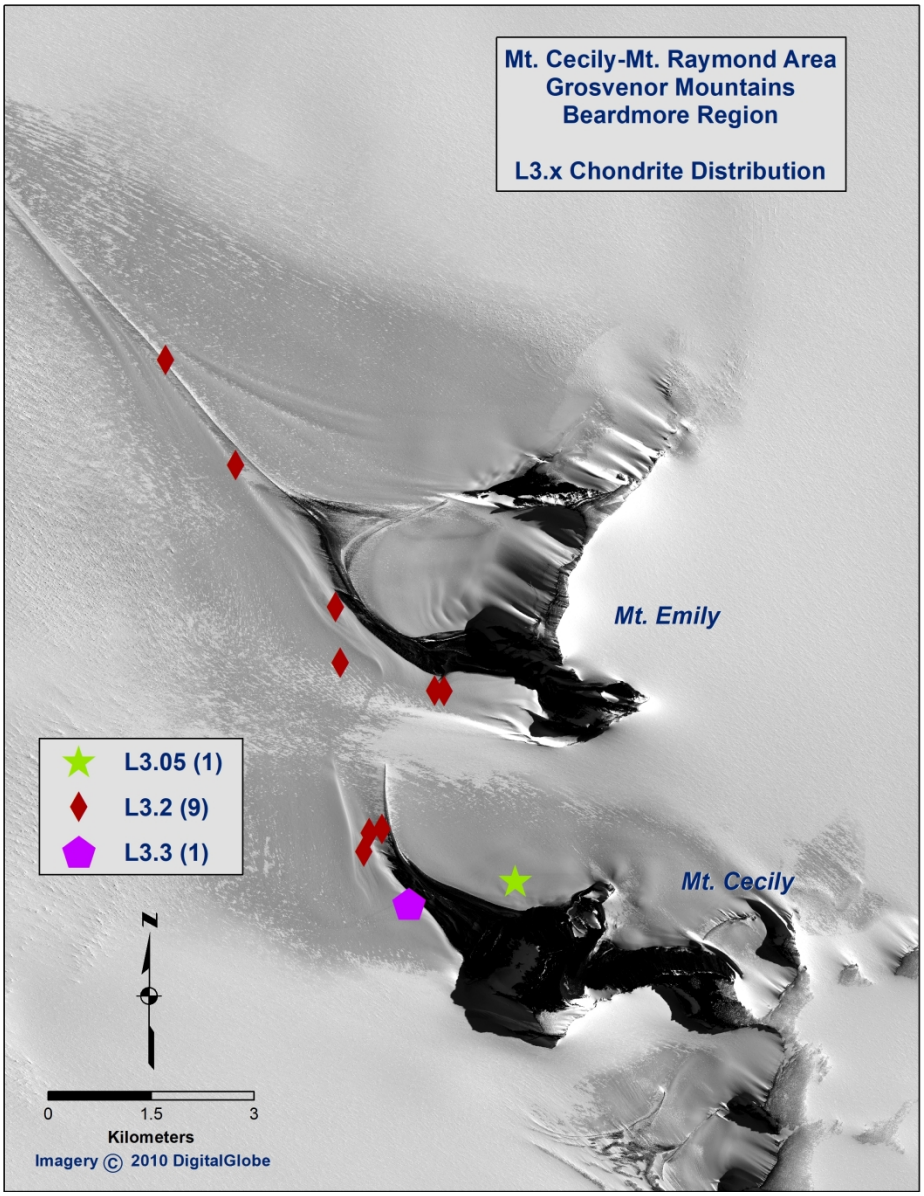

Figure 4b

215x279mm (300 x 300 DPI)

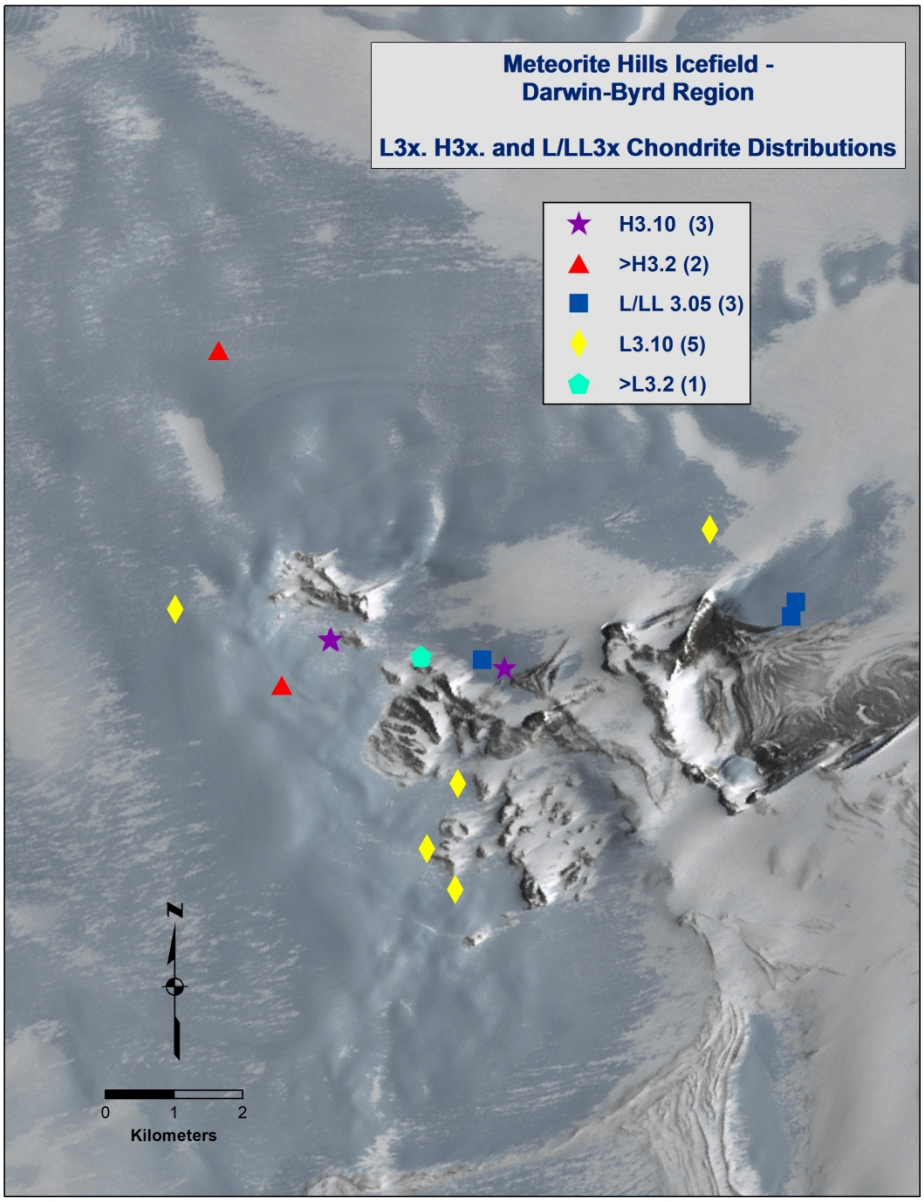

Figure 5

215x279mm (300 x 300 DPI)

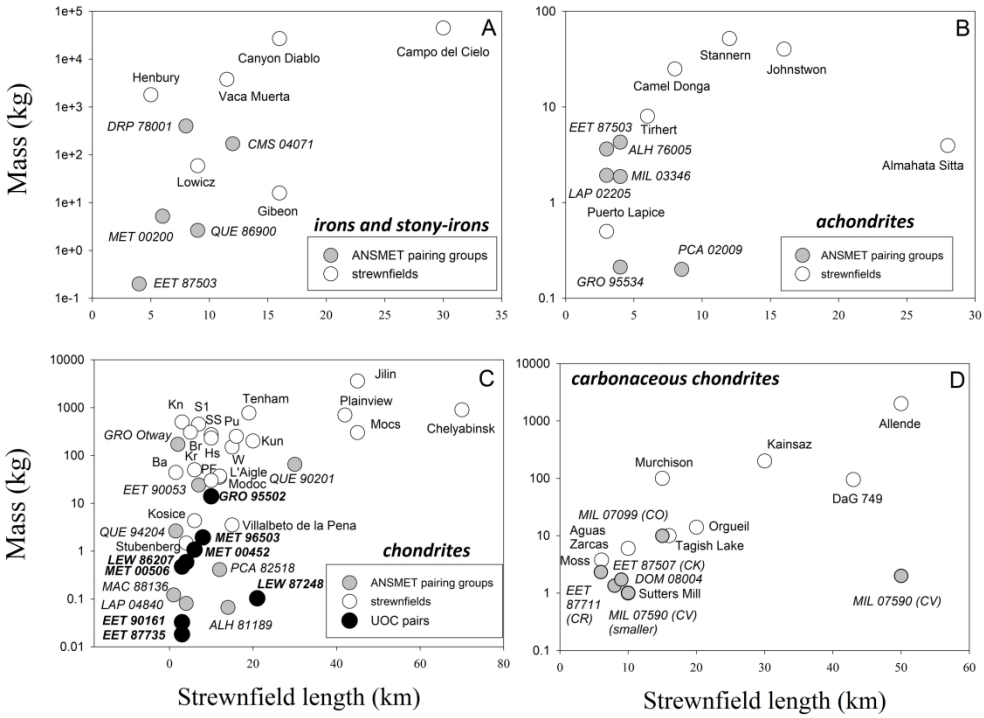

Figure 6

279x215mm (300 x 300 DPI)